3D Printing of Flexible Liquid Sensor Based on Swelling Behavior of Hydrogel with Carbon Nanotubes

*Xiangjia Li, Yang Yang, Benshuai Xie, Ming Chu, Haofan Sun, Siyang Hao, Yiyu Chen, and Yong Chen**

Flexible sensors with accurate detection of environmental stimuli (e.g., humidity and chemical substances) have drawn increasing research interests in biomedical engineering and environmental science. However, most work is focused on isotropic sensing of liquid occurrence due to the limitation of material development, sensor design, and fabrication capability. 3D printing is used to build multifunctional flexible liquid sensors with multimaterials enabling anisotropic detection of microliquid droplets, and described herein. Electrical conductive composite hydrogels capable of detecting chemical liquid are developed with poly (ethylene diacrylate) (PEGDA) and multiwalled carbon nanotube (MWCNT). Due to the absorption of the liquid droplet and related swelling behavior, the resistance of PEGDA/MWCNT composite hydrogel increases dramatically, while the resistance of pure PEGDA hydrogel decreases significantly. Based on the two composite hydrogels and the related 3D printing method, a mesh-shaped liquid sensor that can effectively identify the position and volume of liquid leakage in a short time is developed. Furthermore, a three-layered liquid sensor to enable bidirectional monitor and detection of the liquid leakage in two different sides is demonstrated. The 3D-printed liquid sensor offers a distinctive perspective on the potential applications in various fields for detection of liquid leakage in accurate position and direction.

1. Introduction

Recently, there has been growing interests in wearable electronics and flexible sensors due to instrumentation necessities in engineering subareas, such as transportation, batch manufacturing, energy industry, optical metrology, and biomedical monitoring.[1–3] Various kinds of sensors have been developed to react upon environmental stimuli, for example, the pressure,[4–6] temperature,[2,3] motion,[7] bending,[8,9] gas flow,[10] humidity,[11] chemical liquid,[12–16] and food safety parameters.[2] Traditionally, most sensors were manufactured by solution casting,[11] melt spinning,[13] compression moulding,[14] solution casting,[16] etc. For instance, the solution-casting process was employed to fabricate porous ionic membrane as a humidity sensor, enabling the measurement of water contents of human skin.[11] However, due to geometric complexity, material limitation, and manufacturing restriction, traditional manufacturing methods are usually insufficient to the fabrication requirements of flexible sensors associated with complex geometric shape and multifunctional materials.[2,3,17] Recently, a variety of 3D printing methods, such as stereolithography (SL),[4] inkjet printing,[8] and directed ink writing[9] have been introduced and applied to fabricate sensors in a faster, cheaper, and more customized way.[2,3,17] The development of 3D printing processes has brought us many opportunities in producing next-generation flexible sensors with high efficiency and accuracy.[13,16,17] For instance, a helical-shaped 3D liquid sensor fabricated by solvent-cast 3D printing process can obtain higher electrical conductivity and faster response time compared with the traditional 2D flat surface liquid sensor.[13] In addition, a vast array of materials, including metal, ceramic, polymer, and multiple groups of composite inks, can be processed using 3D printing technologies.[2,3,17] Among them, hydrogel has got considerable interest in the field of flexible sensors, due to its multiple attractive properties, such as swelling effect, biocompatibility, stretch ability, and shape forming ability.[2,3,16,18–25] The swelling behavior of hydrogel in dry and wetting conditions qualitatively shows stimuli-responsive toward chemical liquids.[20,21] After adding conductivity fillers, e.g., ionic compound[4,22] and carbon nanotube,[26] into the hydrogel solution, the nonelectrical shape changes of the hydrogel can be converted into a quantitative electrical signal, drastically improving the chemical sensitivity of pure hydrogel.[21] Therefore, composite hydrogel with electrical conductive fillers can be a potential candidate for the development of flexible sensors.[2,3,17,21,22,26] Although

X. Li, Dr. Y. Yang, Prof. Y. Chen
Epstein Department of Industrial and Systems Engineering
University of Southern California
Los Angeles, CA 90089-01932, USA
E-mail: yongchen@usc.edu

B. Xie, S. Hao, Y. Chen, Prof. Y. Chen
Department of Aerospace and Mechanical Engineering
University of Southern California
Los Angeles, CA 90089, USA

M. Chu, H. Sun
Mork Family Department of Chemical Engineering & Material Science
University of Southern California
Los Angeles, CA 90089-1211, USA

DOI: 10.1002/admt.201800476

composite hydrogels based liquid sensors have already provided a variety of potential applications, most sensors are isotropic and have limitations to accurately distinguish the position or the incoming direction of stimuli.[12–15,27] In addition, liquid sensors have to be immersed into the liquid to detect the volume or distinguish the type of liquid in terms of chemical substances and is hard to detect microsized liquid leakage using traditional liquid sensor.[12–15,27]

Notably, nature provides inspirations to the development of flexible sensor in many ways, such as functional material investigation, structural design methodologies, and unique sensing mechanisms.[6,28–32] Compared with traditional sensors, the sensors with special biomimicking design show higher efficient sensitivity and have profoundly enlightened an approach in the field of smart sensor development.[32–35] For example, animals' whisker perform as a tactile sensor that can detect wind from all directions; based on the bioinspired electronic whisker, a real-time multiple dimensional gas-flow sensor was developed, which is made by high-aspect ratio elastic fibers coated with carbon nanotubes and silver nanoparticles.[34] In addition, creatures in nature are able to keep track of the slight moisture change in the living environment.[27] The moisture sensitivities of human and animal ultimately attribute to the tiny hair above the surface of the skin, which are strongly hygroscopic and can change the shape with the variation of air moisture accurately.[36–39] For instance, the strands of human hair can be used as a hygrometer because of its special composition called keratins, of which the chemical bonds can strand its strength response to the humidity change (refer to **Figure 1**a).[36,37] As the predominant proteins in hair, keratins are easily broken by water due to the interaction of hydrogen molecules; hence, the hair is lengthened with the increasing of humidity and shrunk as the water evaporate out (refer Figure 1b).[37,39]

Inspired by the humidity sensing of human hair, we developed composite hydrogel based on poly (ethylene diacrylate) (PEGDA) and multiwalled carbon nanotube (MWCNT), of which the electrical conductivity is adjusted by controlling the swelling behavior of the hydrogel via absorption of liquid. As shown in Figure 1c, the resistance of the top layer (pure PEGDA) is reduced due to electron transport by absorbed water molecules (Figure 1d). However, the resistance of the bottom layer (PEGDA/MWCNT) is increased due to the incremental distances between MWCNT by the swelling behavior under liquid absorbency (Figure 1e). To fabricate liquid sensor in a highly coherent manner, a multimaterial 3D printing process was developed based on high-resolution stereolithography,[40] and after the printing process, the conductive PEGDA-based composite hydrogel was formed into a resistive sensing element. The electrical conductivity performance of 3D-printed spark shaped PEGDA/MWCNT-based hydrogel was studied in this research. Based on the study, the mesh-shaped sensor was developed to identify the position of liquid leakage. In order to produce a bidirectional liquid sensor for microdroplet, a three-layered artificial hair was further designed with pure PEGDA and PEGDA/MWCNT composites to distinguish the liquid leakage from two sides (Figure 1c). Due to the unique directional sensing, this three-layered liquid sensor has multiple potential applications, such as disease detection, microfluid monitor, and multiscale actuator.[33,41–45]

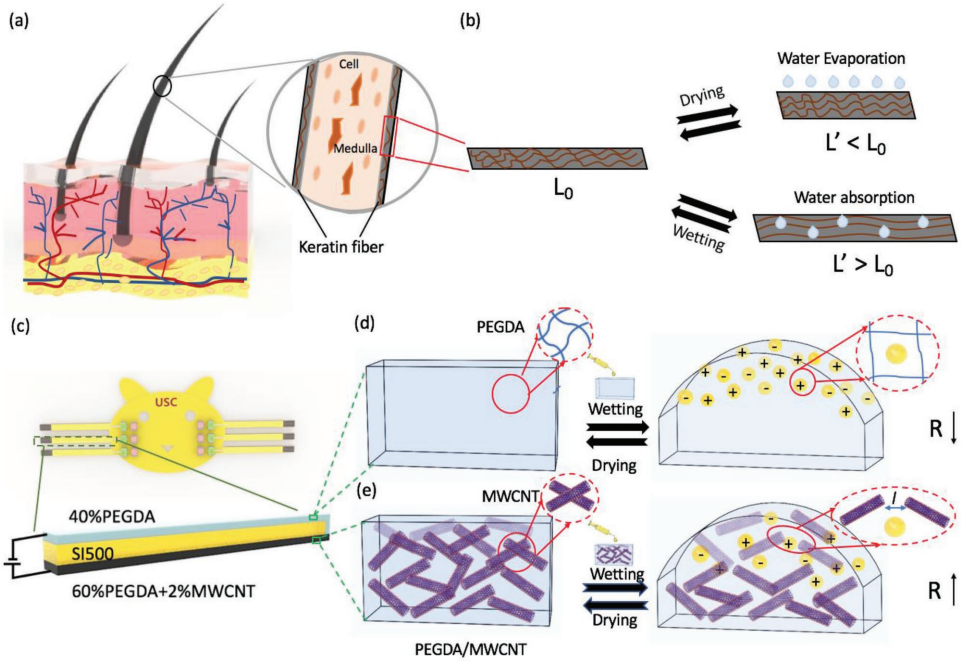

Figure 1. Schematic representation of hair inspired liquid sensor made by PEGDA/MWCNT composite hydrogel. a) Schematic graph of hairs on the surface of human skin; b) the work principle of hair used in hygrometer to monitor the humidity; c) diagram illustration of hair inspired three-layered liquid sensor; d) the conductivity of PEGDA hydrogel by swelling behavior in wetting and drying state; and e) the conductivity of PEGDA/MWCNT composite hydrogel by swelling behavior in wetting and drying state.

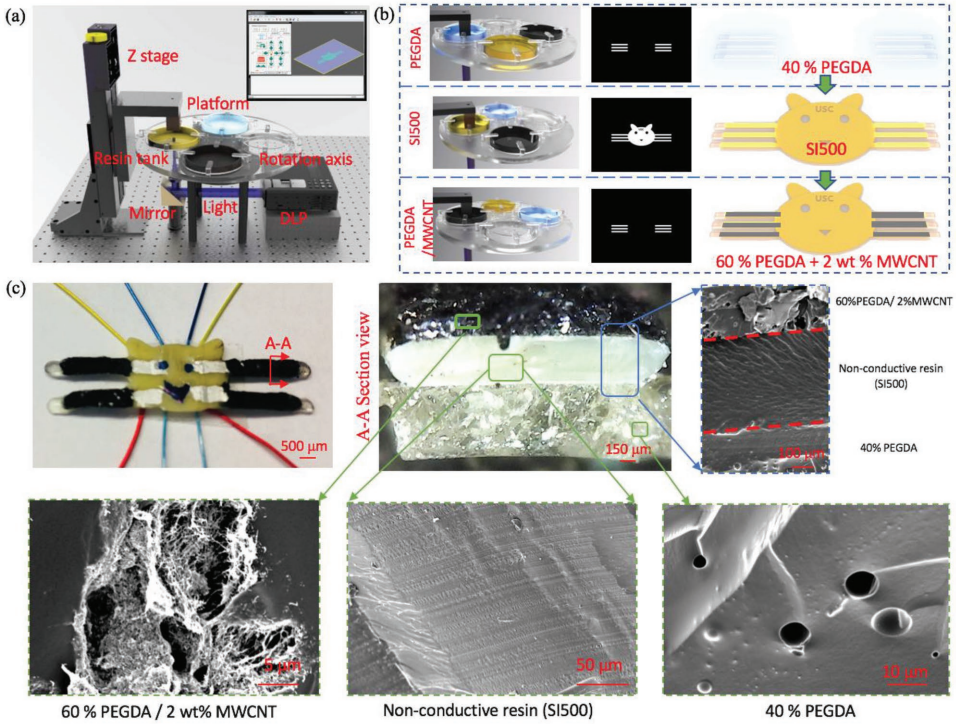

Figure 2. Schematic representation and fabrication result of three-layered liquid sensor by multimaterial MIP-SL. a) Schematic diagram of multimaterial MIP-SL printing prototype machine; b) the slicing and printing process of each layer with different material using the multimaterial MIP-SL; and c) the 3D-printed bidirectional liquid sensor with PEGDA/MWCNT-based composite hydrogel as well as the scanning electron microscope images of each layer of 3D-printed liquid sensor.

2. 3D Printing of PEGDA-Based Composite Hydrogel

The PEGDA hydrogel is a photosensitive material, whose monomers molecules can form complex polymer chains following the initiation by the absorption of ultraviolet (UV) light. Here, a multimaterial mask image projection-based stereolithography (MIP-SL) 3D printing method (**Figure 2**a) is used to accurately cure PEGDA-based composite materials in the corresponding position with high resolution and fast speed.[46–47] The curing property of the PEGDA/MWCNT-based composite hydrogel is shown in Figure S1a in the Supporting Information. The light penetration depth of PEGDA-based hydrogel is reduced dramatically with the addition of MWCNT, and it takes much longer time to solidify the composite hydrogel with the high concentration of MWCNT and low concentration of PEGDA (refer to Figure S1a in the Supporting Information). Thus, 40% PEGDA hydrogel and 60% PEGDA with 2 wt% (weight percentage) MWCNT were used in this work to fabricate the liquid sensors. To demonstrate the ability to fabricate liquid sensors with customized and complex shape, a liquid sensor array in the shape of a cat's head was designed and fabricated. In the printing process, the digital model of liquid sensor array was first sliced into a series of 2D patterned mask images (refer to Figure 2b). Accordingly, the UV light was projected on the bottom surface of the resin, and the first layer of the liquid sensor was fabricated using 40% PEGDA hydrogel. In order to generate a conductive loop of two different connective hydrogels, an additional layer of PEGDA with the smaller area was designed and fabricated. The exposure time when fabricating the first two layers with 40% PEGDA hydrogel at the thickness of 200 μm was 20 s per layer. At the same layer, the rest area of the sensor array (refer to Figure 2b) was cured by an electrical nonconductive material (SI500 from Envisiontec Inc., Michigan, USA). Before curing different materials, the residual resin attached on the precured part need to be cleaned using alcohol.[48] After cleaning, the printed part was moved into a new material reservoir containing SI500, and a layer of SI500 at the thickness 200 μm was solidified under sufficient light exposure time of 2 s per layer. Similarly, the third layers of 60% PEGDA/2 wt% MWCNT with the thickness of 75 μm (30s) were built on the top surface of SI500 layer using the same projection image of the first layer. Using the 3D printing method, multimaterial liquid sensors in various shapes and designs (Figure 2c) can be fabricated into a single component with integrated functions.

3. Results and Discussion

3.1. Liquid Sensitivity of PEGDA/MWCNT-Based Composite Hydrogel

PEGDA-based hydrogel is a network of polymer chains that undergoes volumetric change upon solvent absorption and is capable of accommodating large deformation with microliquid and can swell up to more than five times of its original volume.[49] The resistance of PEGDA hydrogel decreases from several megohms to thousands of ohms due to the dissolved

water-based electrical conductive solvent. For PEGDA/MWCNT composite hydrogel, the resistance increases with the distance between each MWCNT because of the swelling of PEGDA polymer chain. Therefore, the electrical conductivity performance of PEGDA-based hydrogel is mainly determined by the swelling deformation and absorbency capability. The swelling deformation of hydrogel is associated with the resistance change at different diffusion level of microliquid, and the absorbency capability of hydrogel determines its largest alteration in resistance. In the following study, we presented a series of experiments to understand the swelling behavior as well as the electrical conductivity performance of PEGDA-based composite hydrogel.

3.1.1. Swell Behaviors

PEGDA hydrogel presents the hydrophilicity because of the presence of hydrophilic functional groups in the polymeric backbone, and its stability to hold water is due to the crosslinks established between the network chains.[48–51] The swelling deformation of PEGDA-based composite hydrogel was studied (refer to **Figure 3**a–f) (see Experimental Section in the Supporting Information). Based on the Flory–Huggins mixing theory, the isotropic swelling of hydrogel is related to the polymer crosslink ratio and its mechanical stress.[52,53] Higher concentration of PEGDA in the hydrogel solution results in larger mechanical stress, and the addition of MWCNT also improves the mechanical strength (Figure S1b, Supporting Information). As shown in Figure 3b,c, the microdroplet penetrated through the 3D cross-linked network of PEGDA-based hydrogel from the top surface of the test bar and caused the deformation of hydrogel in consequence. The distance between each MWCNT is increased with the gradient permeation of liquid. The thickness of the test bar affects the physical deformation of hydrogel during the swelling process. As shown in Figure 3d, the deformation of the test bar of the thin film is much larger than the thick film, since the thinner layer is more prone to deform under the same bending force. Furthermore, the relative length change $\frac{\Delta l}{l}$ of the test bar is reduced to 0.6–0.8 of the original value after adding 2 wt% MWCNT, because the addition of MWCNT introduces more restrictions on the deformation of hydrogel under the same bending force. With the decreased loading of PEGDA in the composite hydrogel solution, the relative length change of the test bar increased dramatically (refer to Figure S2a in the Supporting Information), and the tendency of the relative length change decreases with the thickness of the hydrogel bar. Since the solvent has unique Flory interaction parameter, the swelling deformation of hydrogel is also determined by the type of the solvent (refer to Figure S2b in the Supporting Information).[48,49] During the liquid diffusion, the hydrogel transits from unsolvated glassy or partially rubbery state to a relaxed rubbery state, and it will change back to glassy state after the absorbed solvent evaporates out.[49] The reversible swelling/deswelling process of PEGDA hydrogel was demonstrated in the Fourier transform infrared (FTIR) spectroscopy (Figure S3, Supporting Information) and reveals the principle that supports the design of the liquid sensor.

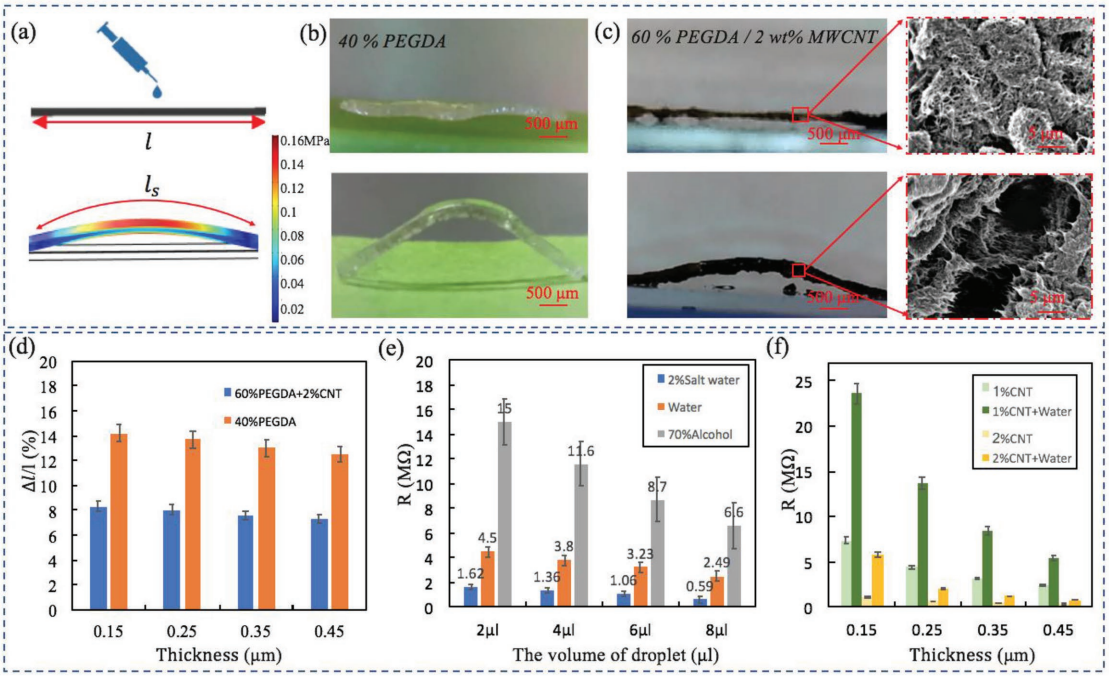

Figure 3. The swelling behaviors and electrical conductivity of PEGDA-based composite hydrogel. a) The schematic representation of swelling deformation of hydrogel; b,c) swelling deformations of 40% PEGDA hydrogel and 60% PEGDA/2 wt%MWCNT hydrogel after absorption of 4 μL water, respectively; d) the relative length change of PEGDA-based hydrogel after absorption of 4 μL water; e) the electrical resistance change of 40% PEGDA hydrogel after absorption of three different kinds of liquid (2% salt water, water, and 70% alcohol); and f) the electrical resistance of 60% PEGDA/2 wt%MWCNT composite hydrogel with different thickness after absorption of 2 μL of water.

The absorbency capability of hydrogel at equilibrium can be measured by the weight change ratio of hydrogel Q_a, which is calculated by the following equation:

$$Q_a = \frac{W_s - W}{W}, \quad (1)$$

where W_s is the swollen weight and W is the initial weight. Based on the Flory–Huggins mixing theory, the absorbency capability of hydrogel at equilibrium is determined by the concentration and the crosslink density of polymer.[50] The absorbency capability of hydrogel with low concentration is larger than the one with a high concentration due to low crosslink density (Figure S2c, Supporting Information). As a result, 40% PEGDA hydrogel shows the largest absorbency capability, with the weight of absorbed water being two times of its original weight. In addition, the mixture of MWCNT has no significant effect on the weight change ratio of PEGDA-based hydrogel (Figure S2c, Supporting Information).

3.1.2. Electrical Conductivity Performance of PEGDA Hydrogel

The electrical conductivity performance of PEGDA hydrogel is expected to be enhanced by the absorption of electrical conductive solvent. To verify this hypothesis, the electrical conductivity of PEGDA hydrogel was tested under different swelling states (refer to Figure 3e). With gradual diffusion of water droplet from 0 to 18 µL, the resistance of 40% PEGDA hydrogel decreases sharply, dropping from 38 MΩ to 17 kΩ. The relative resistance change R_{rel} of PEGDA hydrogel can be calculated by the following equation:

$$\mathrm{R}_{rel} = \frac{R_t - R_s}{R_s}, \quad (2)$$

where R_t is the resistance of hydrogel at time t, and R_s is the resistance of hydrogel at the equilibrium state.

3.1.3. Electrical Conductivity Performance of PEGDA/MWCNT Composite Hydrogel

The electrical conductivity performance of PEGDA/MWCNT composite hydrogel is opposite to PEGDA hydrogel at the same stimuli condition. Due to the swelling with solvent absorption, the distance between MWCNT network in the PEGDA matrix increases (refer to Figure 3c), resulting in the increment of resistance. Even though the diffusion solvent is electrical conductive liquid, the resistance of PEGDA/MWCNT composite is mainly determined by the MWCNT network. The electrical resistance of PEGDA hydrogel was quartered by adding 1wt% MWCNT. The resistivity of 60% PEGDA hydrogel reduces from 1.5 kΩ·m to 21.6 Ω·m by adding 2 wt% MWCNT (Figure 3h). After the diffusion of 2 µL water, its resistivity increases to 116 Ω·m. The resistance change R_{rel} of PEGDA/MWCNT composite hydrogel is calculated by the equation:

$$\mathrm{R}_{rel} = \frac{R_t}{R_o} \quad (3)$$

where R_t is the resistance of PEGDA/MWCNT composite hydrogel at time t, and R_0 is the original resistance of PEGDA/MWCNT composite hydrogel after printing. The resistance change R_{rel} of 60% PEGDA/ 2 wt% MWCNT composite presents declining trend (5.73 for 150 µm thickness to 2.17 for 450 µm thickness with 2 µL water) with the increase of its thickness (refer to Figure 3i). This is attributed to the volume change ratio k_v of hydrogel decreases with the increase of thickness due to Flory–Huggins mixing theory. In addition, the resistance change R_{rel} of PEGDA/MWCNT-based composite hydrogel turns to be smaller with the increase of PEGDA concentration in the composite hydrogel solution.

3.2. 3D-Printed Liquid Sensor for Microdroplet

3.2.1. 3D-Printed Spark-Shaped Liquid Sensor

Based on the aforementioned conductivity studies of PEGDA and PEGDA/MWCNT-based composite hydrogels, spark-shaped liquid sensors was designed and fabricated with 40% PEGDA hydrogel and 60% PEGDA/2 wt% MWCNT, respectively. The resistance of spark-shaped liquid sensor made by 40% PEGDA hydrogel is 3 MΩ, resulting in weak current passing through a connected light-emitting diode (LED) (refer to **Figure 4**a). After 4 µL water was dropped on the surface of this liquid sensor, the resistance of 40% PEGDA gradually reduces to 1.17 MΩ, allowing sufficient current within circuit so that the blue LED was flashed, with the light intensity of LED reaching 28 mw mm^{-2}. After the internal liquid evaporated out from the polymer network and the sensor recover to the original state, 8 µL water was then exerted on this liquid sensor, the resistance declined to 0.477 MΩ within 2 min (Figure 4b). The LED turned to be brighter with light intensity at 60 mw mm^{-2} (Figure 4a). When the volume of water exerted increases to 12 µL, the resistance drops to 5 kΩ with a resistance change of 600 times as shown in Figure 3b.

The liquid sensing performance of spark sensor made by 60% PEGDA/2 wt% MWCNT is different. The resistance of spark rises from 770 kΩ to 10.3 MΩ in 1.2 min with the absorption of 4 µL water, and as a result the light intensity of blue LED drops from 10 to 0.05 mw mm^{-2}. Similarly, the resistance of the third spark strip increases to 17.25 MΩ in 1.8 min after absorbing 8 µL water. When the volume of liquid reaches 12 µL, the resistance change R_{rel} rises from 21 to 33 times and the LED darkened gradually till fully off. Generally, the 3D-printed spark-shaped strips made by 40% PEGDA and 60% PEGDA/2 wt% MWCNT hydrogel present opposite performances upon liquid engagement. That is 40% PEGDA hydrogel presents negative response (resistance reduction) to the microliquid droplet, while the 60% PEGDA/2 wt% MWCNT hydrogel shows positive response (resistance increment) to the microliquid droplet.

3.2.2. 3D-Printed Mesh-Shaped Liquid Sensor

Taking advantage of the liquid sensitivity of PEGDA hydrogel, a mesh-shaped liquid sensor was 3D printed using 40% PEGDA hydrogel as shown in **Figure 5**. This mesh sensor has the capability of identifying where the microliquid is dropped

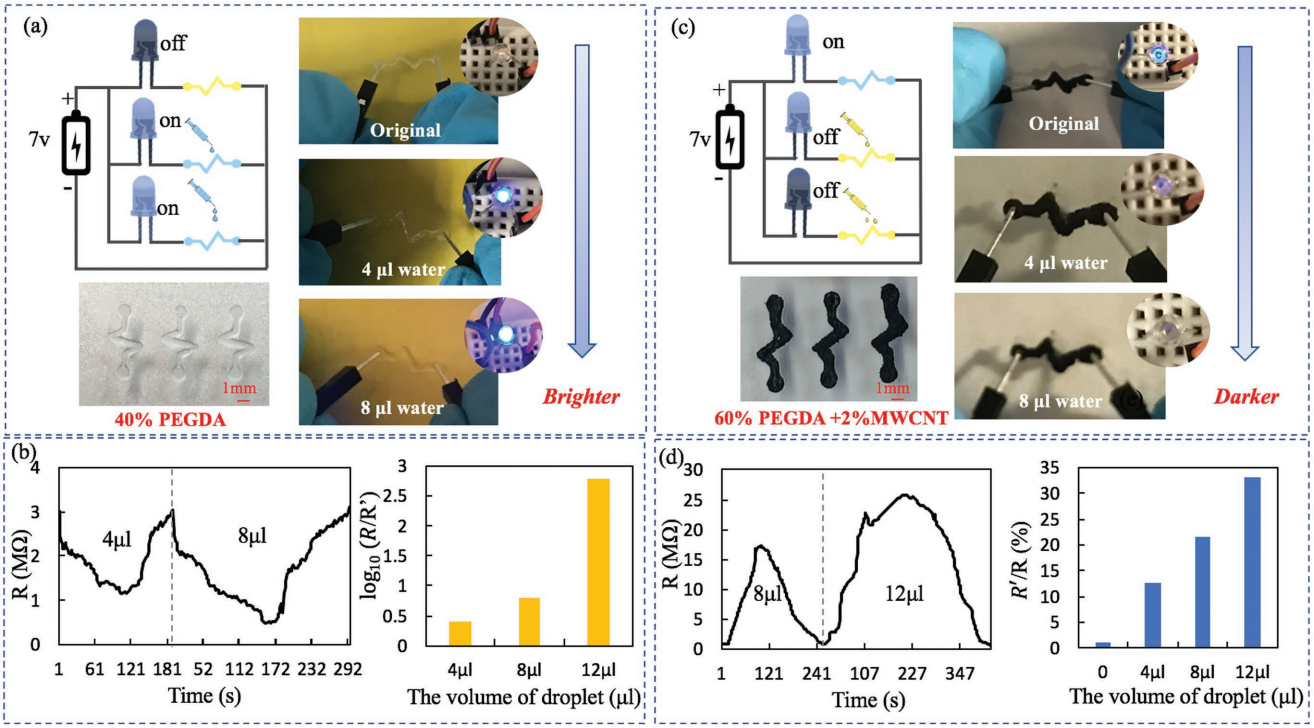

Figure 4. The 3D-printed spark-shaped microliquid sensor with PEGDA hydrogel and PEGDA/MWCNT composite hydrogel. a) The electrical sensitivity test of spark-shaped microliquid sensor with 40% PEGDA hydrogel; b) the resistance change of liquid sensor made by 40% PEGDA hydrogel; c) the electrical sensitivity test of spark-shaped microliquid sensor with 60% PEGDA/2 wt% MWCNT composite hydrogel; and d) the resistance change of liquid sensor made by 60% PEGDA/2 wt% MWCNT composite hydrogel.

on the sensor based on the resistance change of each branch. To demonstrate the concept, the sensor with three branches in each direction was designed and fabricated. First, three bottom branches (4, 5, 6) were printed in the horizontal direction. Then, we fabricated another three branches (1, 2, 3) on the top of them in a perpendicular direction (Figure 5a). Similarly, the stimuli of microliquid wetting on the intersection are easy to be located with the resistance change of these branches. When water (4 µL) was dropped on the cross-section of branches 2 and 5, the related resistance of branch 2 first declines from 1.06 to 0.43 MΩ. As the water continuously penetrated from the top layer to the bottom layer, the resistance of branch 5 is then reduced from 1.176 to 0.621 MΩ. Consequently, the corresponding LEDs connected with both branch 2 and 5 are activated in sequence, and because of the evaporation the blinking LED connected with branch 2 was also turned off earlier than the one connected with branch 5, indicating the position and direction (from top) of microdroplet leakage (Figure 5b). In addition, this mesh-shaped sensor was tested by dropping microliquids at the cross-sections of branch 1 and 4 as well as branch 2 and 6, respectively. The resistance change of branch 2 during the test is shown in Figure 5c, and the response and recovery time was close to 1.5 and 3 min, respectively. The resistance change of the branch that the water first penetrated is slightly higher than the one that water diffused into (Figure 5d). This is because the amount of water reduced after penetration into the bottom layer. The different resistance change of each branch enables the use of this mesh sensor to quantitatively identify where and when microdroplet contact the sensor as well as estimate its volume.

3.2.3. Hair Inspired Liquid Leakage Sensor

In order to detect the bidirectional leakage of microliquid using a sensor, the hair inspired liquid leakage sensor array was designed and printed by multimaterial MIP-SL approach (**Figure 6**a). In hair inspired liquid sensor, the two outmost electrical conductive layers were printed using negative liquid sensitive 40% PEGDA hydrogel and positive liquid sensitive 60% PEGDA/2 wt% MWCNT composite hydrogel, respectively. To create an electric loop with these two electrical conductive layers, an insulation layer is added between the pure PEGDA and PEGDA/MWCNT composites (refer to Figure 1c), and the current goes through the sensor from the up to the bottom layer. When the resistance of the hair inspired sensor decreases, the red LED will be lightened, whereas the green LED will be turned on when the resistance increases. Spreading 4 µL water on the top surface of the transparent layer made by 40% PEGDA hydrogel is performed to test the leakage detection capability. The results show its resistance reduces from 8.6 to 6.9 MΩ, triggering the red LED to light up and alarm rings (Figure 6b,c). After the internal water evaporated out, another 4 µL water was dropped on the bottom side of 60% PEGDA/2wt% MWCNT composite. The resistance of the hair inspired sensor dramatically increases to 11.6 MΩ, and the green LED is lightened and the alarm rings (refer to Figure 6b,c). The different reaction of resistance changes upon water dropping from different sides of the sensor is utilized to indicate the direction the leakage comes from. The sensor array, consisting a certain count of the aforementioned sensor unit, is achieved with a

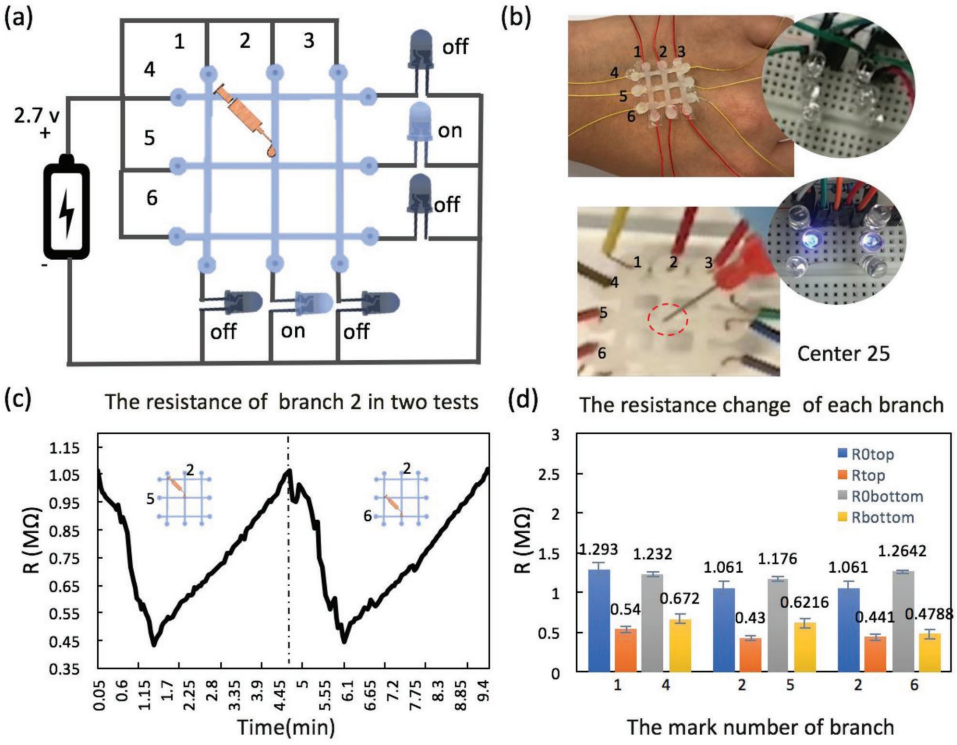

Figure 5. The 40% PEGDA hydrogel-based liquid sensor printed by MIP-SL process. a) The circuit diagram of mesh-shaped microliquid sensor; b) the electrical sensitivity test of mesh-shaped liquid sensor after absorption of 4 µL water; c) the electrical resistance change of branch 2 after diffusion of 4 µL water in two tests; and d) the resistance changes of each branch during the electrical sensitivity test.

design inspired by the human hair. Compared with the traditional sensor, the flexible hair inspired sensor array covers more area with the same material consumption and accurately detects a large range of microliquid leakage that spans from 0.1 to 1 µL mm^{-2}. Meanwhile, it achieved precise localization of microfluid leakage with the capability of identifying liquid from both directions, revealing potential applications in microfliud sensing and multiscale actuator.[41–45]

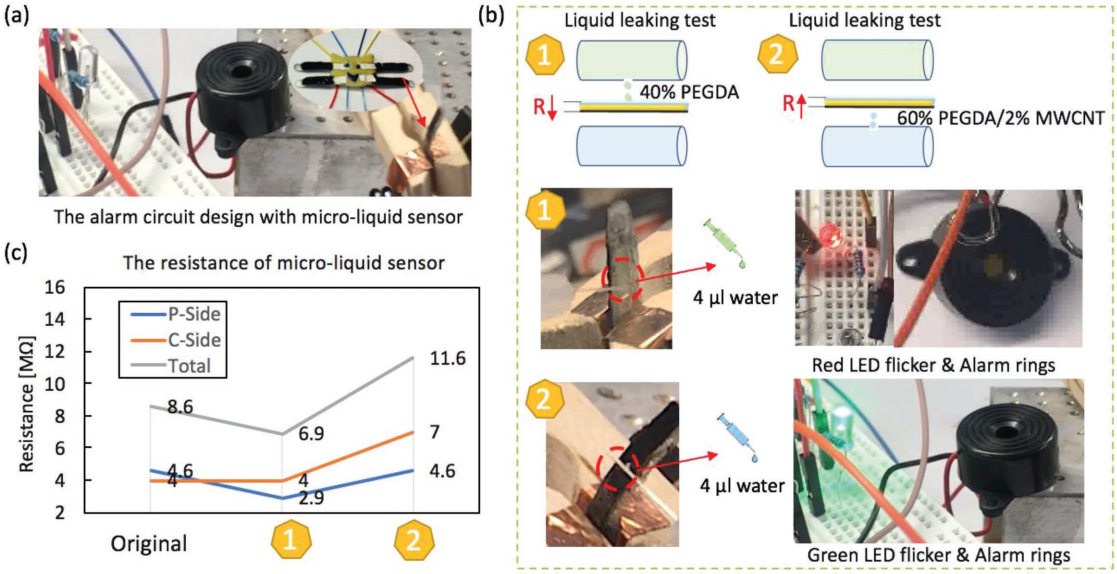

Figure 6. The hair-shaped liquid sensor printed by the multimaterial MIP-SL printing process. a) The microliquid leakage detection circuit with the hair-shaped liquid sensor, LED, and alarm; b) the microliquid detection of the hair-shaped sensor made by 40% PEGDA hydrogel and 60% PEGDA/2 wt% MWCNT composite hydrogels; and c) the electrical resistance change of the 3D-printed hair-shaped microliquid sensor after absorption of 4 µL water.

4. Conclusion

In the paper, we studied the 3D printing of liquid sensors with the capability of detecting the accurate position and direction of liquid leakage. The resistance change of PEGDA hydrogel transformed from negative to positive at the same wetting condition after adding MWCNT in PEGDA hydrogel. In addition, the response and recovery time of PEGDA/MWCNT-based hydrogel sensor is associated with the testing solvents. We demonstrated the repeatability and reliability of 3D-printed liquid sensor for microdroplet, which has a reasonable response time and apparent resistance change (hundreds of times). Based on the study, a mesh-shaped liquid sensor made by 40% PEGDA hydrogel can be used to monitor the wetting condition and identify the position of microliquid. By taking advantage of different liquid sensitivities of PEDGA and PEGDA/MWCNT composite hydrogels, a bioinspired liquid sensor with bidirectional liquid sensitivity has been demonstrated with high efficiency and resolution. In the future, 3D structural liquid sensor with the special distribution of composite hydrogels will designed and fabricated by the MIP-SL process to detect the microliquid in 3D space, which can potentially extend the bidirectional liquid sensing to multidirectional detecting.

5. Experimental Section

Materials: To prepare 40% PEGDA (Mw 700, Sigma-Aldrich) hydrogel solution, the visible light photoinitiator (Irgacure 819, BASF) was used at a concentration of 0.5% (w/v) to induce chain polymerization crosslinking of PEGDA hydrogel by the free radicals. First, the photoinitiator was fully dissolved in the phosphate buffered saline (PBS, Sigma-Aldrich), and then 40% (w/v) PEGDA was gradually added into the above PBS. The 40% PEGDA solution was degassed in the vacuum before usage. 100% (w/v), 80% (w/v), and 60% (w/v) PEGDA solutions were prepared respectively following above procedures. The 60% (w/v) PEGDA/2 wt% MWCNT composite was prepared with dispersion of 2 wt% of noncovalent functionalized multiwalled carbon nanotubes (length (1–5 μm) and outer diameter (5–15 nm), Bucky, USA Inc.) into the 60% (w/v) PEGDA solution. The solution was blended using a global dispersion method. In this method, a magnetic stirrer was used for global agitation for 2 h and ultrasonic with a power of 700 W, frequency of 20 kHz, for 20 min. The composite was degassed in the vacuum before fabrication. Similarly, the above procedures were followed to prepare other PEGDA/MWCNT composite solutions.

Multimaterials MIP-SL: The prototype machine of multimaterial MIP-SL consisted of optical module, material supply module, and motion module.[47] As shown in Figure 2a, the light illuminated and reflected by the Digital Micro-mirror Device, which contained millions of micro mirrors. The reflected light went through the optical lens (f:125 mm, Thorlab) and focused at the bottom surface of the resin tank.[46,54] In the multimaterial MIP-SL, the printing area was 75×42 mm^2, and the resolution of curing light was 40 μm per pixel.[54] Using the multimaterial MIP-SL, liquid sensor array consisted of multiple materials could be directly fabricated by one printing process. In the fabrication, the digital model of liquid sensor was sliced into a series of projection mask images and then based on the material index different kind of materials could be accumulated to form 3D-shaped sensor.[40]

Material Character: The morphology of microstructures was characterized using scanning electron microscope (JSM-7600F, JEOL Ltd). The FTIR spectroscopy testing of hydrogel sample bar at three different states (i.e., normal printed state, dry state, equilibrium swell state) was conducted by Nicolet 4700 with thermal gravimetric analysis/FTIR interface. The mechanical strength of PEGDA/MWCNT-based composite hydrogel was identified using the tension and compression machine (Instron 5492 Dual Column Testing systems, Instron, MA, USA). The swelling tests of PEGDA-based composite hydrogel and the conductivity tests of printed sensor could be seen in the Supporting Information.

Supporting Information

Supporting Information is available from the Wiley Online Library or from the author.

Acknowledgements

The work was partially supported by National Science Foundation (NSF) grant nos. 1151191 and 1663663. The authors also acknowledge the Core Centre of Excellence in Nano Imaging (CNI) at USC for the use of microscopic measuring equipment, and Prof. Steven Nutt and Daniel Zebrine for their help with the FTIR testing.

Conflict of Interest

The authors declare no conflict of interest.

Keywords

3D printing, hydrogel, liquid sensor, multiwall carbon nanotube, swelling

Received: September 26, 2018
Revised: October 23, 2018
Published online:

[1] L. Lin, Y. Hu, C. Xu, Y. Zhang, R. Zhang, X. Wen, Z. Wang, *Nano Energy* **2013**, *2*, 1.
[2] Y. Xu, X. Wu, X. Guo, B. Kong, M. Zhang, X. Qian, S. Mi, W. Sun, *Sensors* **2017**, *17*, 5.
[3] Y. Ni, R. Ji, K. Long, T. Bu, K. Chen, S. Zhuang, *Appl. Spectrosc. Rev.* **2017**, *52*, 623.
[4] M. Vatani, M. Vatani, J. W. Choi, *Appl. Phys. Lett.* **2016**, *108*, 6.
[5] L. Wang, J. A. Jackman, E. L. Tan, J. H. Park, M. G. Potroz, E. T. Hwang, N. J. Cho, *Nano Energy* **2017**, *36*.
[6] M. L. Jin, S. Park, Y. Lee, J. H. Lee, J. Chung, J. S. Kim, J. S. Kim, S. Y. Kim, E. Jee, D. W. Kim, J. W. Chung, *Adv. Mater.* **2017**. *29*, 1605973.
[7] Y. Yang, B. Zhu, D. Yin, J. Wei, Z. Wang, R. Xiong, J. Shi, Z. Liu, Q. Lei, *Nano Energy* **2015**, *17*.
[8] M. Gao, L. Li, Y. Song, *J. Mater. Chem. C* **2017**, *5*, 12.
[9] J. T. Muth, D. M. Vogt, R. L. Truby, Y. Mengüç, D. B. Kolesky, R. J. Wood, J. A. Lewis, *Adv. Mater.* **2014**, *26*, 36.
[10] J. Wu, K. Tao, Y. Guo, Z. Li, X. Wang, Z. Luo, S. Feng, C. Du, D. Chen, J. Miao, L. K Norford, *Adv. Sci.* **2017**, *4*, 3.
[11] T. Li, L. Li, H. Sun, Y. Xu, X. Wang, H. Luo, Z. Liu, T. Zhang, *Adv. Sci.* **2017**, *4*, 5.
[12] S. Guo, X. Yang, M. Heuzey, D. Therriault, *Nanoscale* **2015**, *7*, 15.
[13] K. Chizari, M. Daoud, A. Ravindran, D. Therriault, *Small* **2016**, *12*, 44.
[14] K. Kobashi, T. Villmow, T. Andres, P. Pötschke, *Sens. Actuators, B* **2008**, *134*, 2.
[15] K. Kobashi, T. Villmow, T. Andres, L. Häußler, P. Pötschke, *Smart Mater. Struct.* **2009**, *18*, 035008.

[16] T. Villmow, S. Pegel, A. John, R. Rentenberger, P. Pötschke, *Mater. Today* **2011**, *14*, 7.
[17] Y. Yang, X. Song, X. Li, Z. Chen, C. Zhou, Q. Zhou, Y. Chen, *Adv. Mater.* **2018**, *30*, 1706539.
[18] L. Pan, G. Yu, D. Zhai, H. Lee, W. Zhao, N. Liu, H. Wang, B. Tee, Y. Shi, Y. Cui, Z. Bao, *Proc. Natl. Acad. Sci. USA* **2012**, *109*, 24.
[19] A. Bhardwaj, I. Shainberg, D. Goldstein, D. Warrington, G. J. Levy, *Soil Sci. Soc. Am. J.* **2007**, *71*, 2.
[20] A. Richter, G. Paschew, S. Klatt, J. Lienig, K. Arndt, H. J. P. Adler, *Sensors* **2008**, *8*, 1.
[21] K. Deligkaris, T. Tadele, W. Olthuis, A. van den Berg, *Sens. Actuators, B* **2010**, *147*, 2.
[22] K. Tian, J. Bae, S. Bakarich, C. Yang, R. Gately, G. Spinks, M. in het Panhuis, Z. Suo, J. Vlassak, *Adv. Mater.* **2017**, *29*, 10.
[23] V. Sridhar, K. Takahata, *Sens. Actuators, A* **2009**, *155*, 1.
[24] Y. Xiang, D. Chen, *Eur. Polym. J.* **2007**, *43*, 10.
[25] F. Zhang, J. Fan, P. Zhang, M. Liu, J. Meng, L. Jiang, S. Wang, *NPG Asia Mater.* **2017**, *9*, 5.
[26] G. Cai, J. Wang, K. Qian, J. Chen, S. Li, P. S. Lee, *Adv. Sci.* **2017**, *4*, 1600190.
[27] J. Huang, J. Wang, A. A. Zhukova, M. N. Rumyantseva, A. M. Gaskov, K. Yu, C. Gu, J. Liu, *Sensor Lett.* **2016**, *26*, 10.
[28] H. Chou, A. Nguyen, A. Chortos, J. To, Lu, C. Mei, J. Kurosawa, W. Bae, J. Tok, Z. Bao, *Nat. Commun.* **2015**, *6*, 8011.
[29] M. Ha, S. Lim, S. Cho, Y. Lee, S. Na, C. Baig, H. Ko, *ACS Nano* **2018**, *12*, 4.
[30] R. Potyrailo, R. Bonam, J. Hartley, T. Starkey, P. Vukusic, M. Vasudev, T. Bunning, R. Naik, Z. Tang, M. Palacios, M. Larsen. *Nat. Commun.* **2015**, *6*, 7959.
[31] G. J. Zeb, K. Y. Su, K. H. Choi, *Soft Rob.* **2018**, *5*, 122.
[32] Y. Yang, X. Li, X. Zheng, Z. Chen, Q. Zhou, Y. Chen, *Adv. Mater.* **2018**, *30*, 9.
[33] K. Takei, Z. Yu, M. Zheng, H. Ota, T. Takahashi, A. Javey, *Proc. Natl. Acad. Sci. USA* **2014**, *111*, 5.
[34] Q. Hua, H. Liu, J. Zhao, D. Peng, X. Yang, L. Gu, C. Pan, *Adv. Electron. Mater.* **2016**, *2*, 7.
[35] M. Tiwana, S. Redmond, N. Lovell, J. Iqbal, *Appl. Sci.* **2016**, *6*, 10.
[36] C. Popescu, H. Höcker, *Chem. Soc. Rev.* **2007**, *36*, 1282.
[37] R. Dawber, *Clin. Dermatol.* **1996**,*14*, 105.
[38] B. Bolormaa, J. Y. Drean, D. Enkhtuya, *J. Nat. Fibers* **2008**, *4*, 1.
[39] M. E. Diamond, M. Von Heimendahl, P. M. Knutsen, D. Kleinfeld, E. Ahissar, *Nat. Rev. Neurosci.* **2008**, *9*, 601.
[40] C. Zhou, Y. Chen, Z. Yang, B. Khoshnevis, *Rapid Prototyping J.* **2013**, *19*, 3.
[41] W. He, Y. Sun, J. Xi, A. A. M. Abdurhman, J. Ren, H. Duan, *Anal. Chim. Acta.* **2016**, *903*, 61.
[42] F. Ju, S. Ling, *Meas. Sci. Technol.* **2013**, *24*, 5.
[43] F. C. M. De Pol Van, J. Branebjerg, *Microsyst. Technol.* **1990**, 799.
[44] J. Chen, H. Guo, J. Zheng, Y. Huang, G. Liu, C. Hu, Z. Wang, *ACS Nano* **2016**, *10*, 8.
[45] L. Alwis, T. Sun, K. T. V. Grattan, *Measurement* **2013**, *46*, 10.
[46] X. Li, H. Mao, Y. Pan, Y. Chen, *ASME 13th International Manufacturing Science and Engineering Conference (MSEC)*, **2018**, V001T01A021, https://doi.org/10.1115/MSEC2018-6708.
[47] X. Li, Y. Chen, *J. Manuf. Process.* **2017**, *28*, 531.
[48] J. Xie, X. Liu, J. Liang, Y. Luo, *J. Appl. Polym. Sci.* **2009**, *112*, 2.
[49] N. C. Padmavathi, P. R. Chatterji, *Macromolecules* **1996**, *29*, 1976.
[50] F. Ganji, S. Vasheghani-Farahani, E. Vasheghani-Farahani, *Iran. Polym. J.* **2010**, *19*, 5.
[51] M. Lesho, N. Sheppard, *Polym. Gels Networks* **1998**, *5*, 6.
[52] M. L. Huggins, *J. Chem.Phys.* **1941**, *9*, 5.
[53] P. J. Flory, *J. Chem.Phys.* **1942**, *10*, 1.
[54] X. Li, B. Xie, J. Jin, Y. Chai, Y. Chen, *Procedia Manuf.* **2018**, *26*, 1023.